New Mexico Geological Society

Downloaded from: https://nmgs.nmt.edu/publications/guidebooks/74

Using InSAR and GNSS observations to investigate verical motions in the Valles Caldera, Northern New Mexico

Savannah C. Devine, Eric Lindsey, Nathan Maier, Ronni Grapenthin, and Andrew Newman, [eds.]
2024, pp. 271-279. https://doi.org/10.56577/FFC-74.271

in:

Geology of the Nacimiento Mountains and Rio Puerco Valley, Karlstrom, Karl E.;Koning, Daniel J.;Lucas, Spencer G.;Iverson, Nels A.;Crumpler, Larry S.;Aubele, Jayne C.;Blake, Johanna M.;Goff, Fraser;Kelley, Shari A., New Mexico Geological Society 74 th Annual Fall Field Conference Guidebook, 334 p.

This is one of many related papers that were included in the 2024 NMGS Fall Field Conference Guidebook.

Annual NMGS Fall Field Conference Guidebooks

Every fall since 1950, the New Mexico Geological Society (NMGS) has held an annual Fall Field Conference that explores some region of New Mexico (or surrounding states). Always well attended, these conferences provide a guidebook to participants. Besides detailed road logs, the guidebooks contain many well written, edited, and peer-reviewed geoscience papers. These books have set the national standard for geologic guidebooks and are an essential geologic reference for anyone working in or around New Mexico.

Free Downloads

NMGS has decided to make peer-reviewed papers from our Fall Field Conference guidebooks available for free download. This is in keeping with our mission of promoting interest, research, and cooperation regarding geology in New Mexico. However, guidebook sales represent a significant proportion of our operating budget. Therefore, only *research papers* are available for download. *Road logs*, *mini-papers*, and other selected content are available only in print for recent guidebooks.

Copyright Information

Publications of the New Mexico Geological Society, printed and electronic, are protected by the copyright laws of the United States. No material from the NMGS website, or printed and electronic publications, may be reprinted or redistributed without NMGS permission. Contact us for permission to reprint portions of any of our publications.

One printed copy of any materials from the NMGS website or our print and electronic publications may be made for individual use without our permission. Teachers and students may make unlimited copies for educational use. Any other use of these materials requires explicit permission.

This page is intentionally left blank to maintain order of facing pages.

New Mexico Geological Society Guidebook, 74th Fall Field Conference, 2024, p. 271–279, https://doi.org/10.56577/FFC-74.271

USING INSAR AND GNSS OBSERVATIONS TO INVESTIGATE VERTICAL MOTIONS IN THE VALLES CALDERA, NORTHERN NEW MEXICO

SAVANNAH C. DEVINE[1], ERIC LINDSEY[1], NATHAN MAIER[2], RONNI GRAPENTHIN[3], AND ANDREW NEWMAN[4]

[1]Department of Earth and Planetary Sciences, Northrop Hall, 221 Yale Blvd. NE, University of New Mexico, Albuquerque, NM 87131; sdevine1@unm.edu
[2]Los Alamos National Laboratory, Bikini Atoll Road, Los Alamos, NM 87454
[3]Geophysical Institute, University of Alaska Fairbanks, 2156 Koyukuk Drive, Fairbanks, AK 99775
[4]School of Earth and Atmospheric Sciences, Georgia Institute of Technology, 311 Ferst Drive, Atlanta, GA 30332

Abstract—The Valles Caldera is a rhyolitic "supervolcano" formed during very large caldera-forming eruptions at 1.231 Ma and expelling ~400 km^3 of ignimbrite, the Tshirege Member of the Bandelier Tuff (Goff, 2010; Nasholds and Zimmerer, 2022). Valles Caldera has a similar structure and composition as other large silicic calderas worldwide, including the Yellowstone and Long Valley Calderas. Understanding whether Valles is currently deforming will allow for a better understanding of any magmatic processes ongoing within the caldera. Here, we present an InSAR time series of the Valles Caldera using 37 interferograms from the Sentinel-1 satellite, spanning 2014 to 2022. We also present preliminary GNSS observations from a survey conducted in October 2022 and compare the results to surveys in 2002 and 2003 to estimate the cumulative deformation over a 20-year period. The InSAR and GPS results show a small signal within measurement uncertainty that broadly suggests subsidence within and around the Valles. We suggest that installation of a continuous GPS network would help better resolve deformation within the caldera and help isolate seasonal signals due to hydrology from signals due to long-term magmatic processes.

INTRODUCTION

Geologic Setting

The Valles Caldera complex (Fig. 1) is a large rhyolitic caldera system, as are the Yellowstone and Long Valley caldera systems (Tizzani et al., 2007; Vasco et al., 2007). The Valles Caldera is part of the Jemez Mountains volcanic field, which has been geologically active for mor than 15 million years (Wolff et al., 2011; Kelley et al., 2013). A caldera-forming eruption at 1.62±0.04 Ma led to the creation of the Toledo Caldera (Spell et al., 1996), which was then followed by Valles at 1.231±0.001 Ma (Nasholds and Zimmerer, 2022). The caldera complex likely formed due to extensional forces at the intersection of the Rio Grande rift (~30 Ma) and the Jemez lineament (Wannamaker, 1997; Goff and Kelley, 2021) and the long-term rise of basaltic to rhyolitic magmas (Kelley et al., 2013).

Most Recent Activity

Between 1.23 and 0.52 Ma, multiple eruptions around the Valles ring fracture zone caused the formation of rhyolitic (high in silica) lava domes and minor tuffs in the caldera (Goff et al., 2011). This was followed by a dormant period of around 460 ka, which ended in the last intracaldera eruption at 68.3±1.5 ka (Zimmerer et al., 2016; Nasholds and Zimmerer, 2022).

^{39}Ar/^{40}Ar dating shows that the youngest eruption at Valles occurred at 68.3±1.5 ka (Zimmerer et al., 2016). This youngest eruption was preceded by the El Cajete Pyroclastic Beds and the Battleship Rock Ignimbrite at 74.4±1.3 ka (Goff et al, 2011; Wolff et al., 2011; Zimmerer et al., 2016). Wolff and Gardner (1995) argued that the Valles Caldera may be entering a new cycle of activity because of mafic magma intrusion in the southern ring fracture zone. Seismic studies dating back to 1981 indicate the presence of a low-velocity zone, which

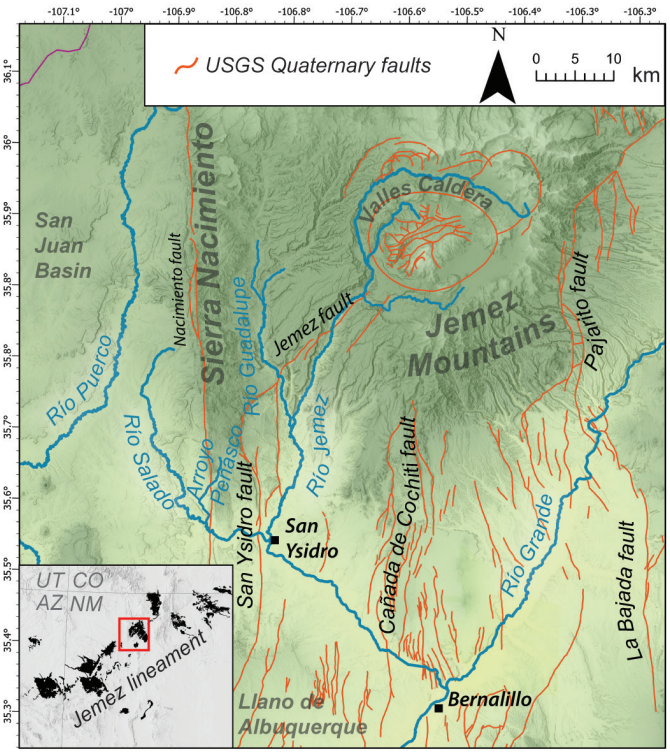

FIGURE 1a. The Jemez region in northern New Mexico, within the Rio Grande rift. The Valles Caldera is indicated, as is the Pajarito fault. *This figure is the work of Cameron Chavez Reed and was used with permission.*

implies the presence of partially liquid magma (Suhr, 1981; Roberts et al., 1991; Steck et al., 1998). The most recent studies have constrained this low-velocity zone to 3–10 km below Redondo Peak (Fig. 1b; Wilgus et al., 2023).

A better understanding of the deformation of this caldera complex would allow for more accurate understanding of the state of the volcanic system. Current geodetic observations across the U.S. Southwest indicate a broad pattern of subsidence at rates less than 1 mm/yr within the Rio Grande rift and part of the Jemez lineament (Berglund et al., 2012; Murray et al., 2019). This may be related to active tectonic deformation within this region and should be considered when observing a more localized deformation source within this area. Faults in the region typically slip at rates less than 0.2 mm/yr (van Wijk et al., 2018). It is hypothesized that the measurable observed deformation is a direct result of ongoing rifting and is not related to some other source of deformation within the caldera (Berglund et al., 2012; Murray et al., 2019).

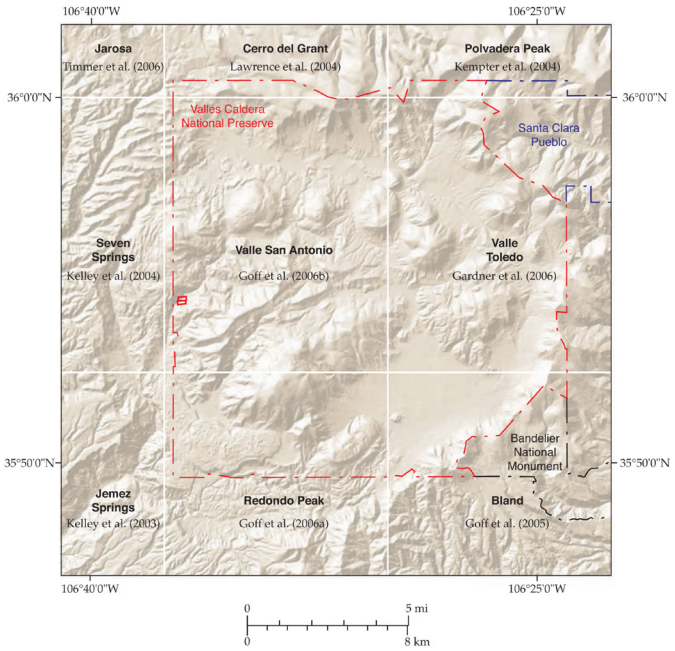

FIGURE 1b. Notable regions within the Valles Caldera complex from Goff et al., 2011.

Use of InSAR

Synthetic aperture radar (SAR) is an active remote sensing method that uses microwaves to image objects and surfaces (Bamler and Hartl, 1998). Interferometric synthetic aperture radar (InSAR) is a method of analyzing SAR imagery by determining the phase differences between two or more precisely aligned SAR images taken from different positions or times to measure topography or deformation, respectively (Bamler and Hartl, 1998). InSAR is commonly used to measure ground deformation over wide areas and can detect movement over timescales of weeks to years. Our study uses data from Sentinel-1 (1-A and 1-B), a European Space Agency satellite mission that collects SAR images every 12 days over much of the world. The effectiveness of InSAR for studying deformation varies due to noise from vegetation, the troposphere, and the ionosphere (Treuhaft et al., 1996; Bekaert et al., 2015; Liang et al., 2019). These errors can contribute to lower accuracy when compared to global navigation satellite systems (GNSS). Moreover, the estimated horizontal motion has lower accuracy due to the "look angle" of the satellite being nearly vertical (Wright et al., 2004).

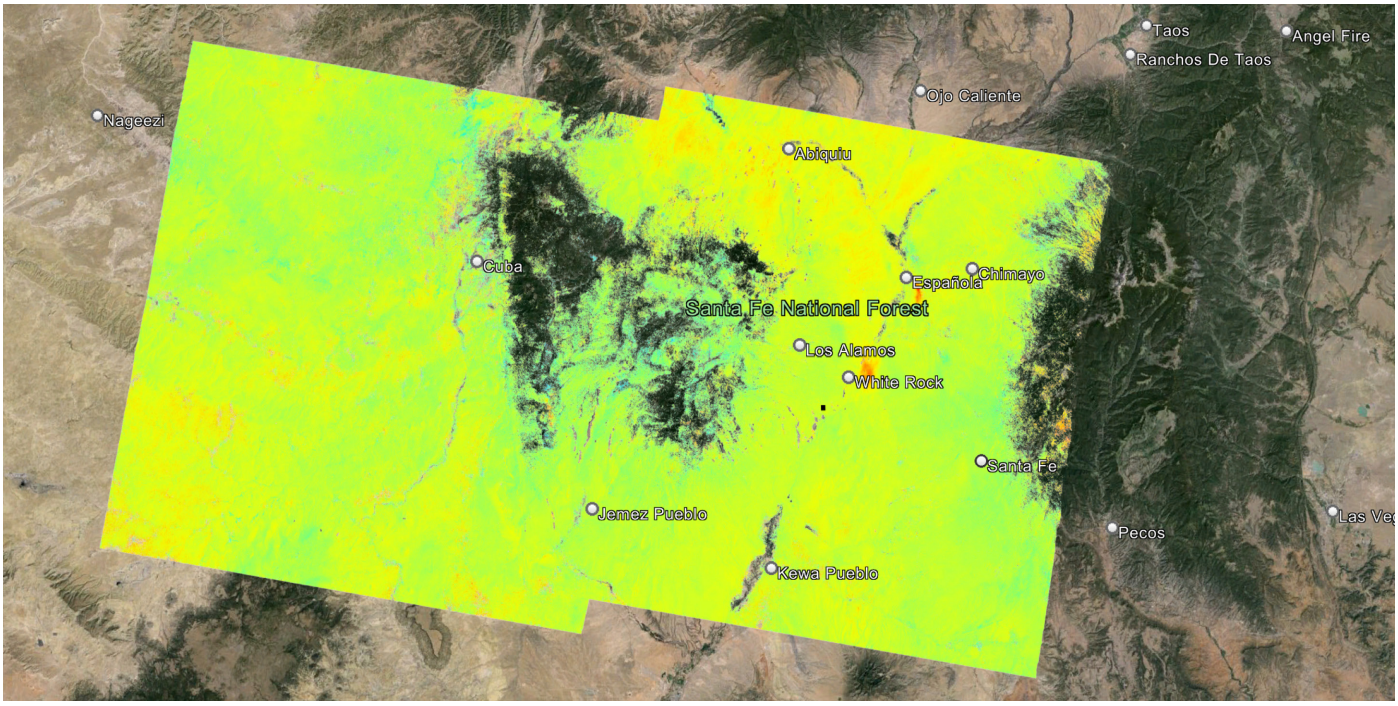

FIGURE 1c. The general Valles Caldera region, with the area we processed using InSAR indicated.

InSAR has been used to observe volcanic deformation since the 1990s, with initial application to Mount Etna in Italy (Massonnet et al., 1995). This method allows for volcano deformation to be mapped across a much larger area and at relatively longer time scales (depending on the mission lifetime of the method used) as compared to other techniques, and it can be used in places where ground monitoring was previously sparse or is too dangerous such as Alaska (e.g., Lu and Dzurisin, 2014; Grapenthin et al., 2022). InSAR is now applied on a much larger scale, with application to both volcanic signals and other types of ground deformation such as fault-related deformation or groundwater motion (Poland and Zebker, 2022). Fialko and Simons (2001) used InSAR to estimate deformation due to the Socorro magma body, which is another volcanic system in the central Rio Grande rift, New Mexico, that remains active to date (Block et al., 2023).

InSAR has previously been used to observe crustal deformation in Yellowstone, a caldera complex similar to Valles Caldera, resulting in a detailed map of subsidence in the region (Dzurisin et al., 1990). By imaging the long-term surface deformation of a region with high spatial resolution, we can better understand the location and depth of the subsurface sources of the motion, significantly improving our hazard modeling of that caldera system. In this study, we used InSAR to estimate the deformation pattern within the Valles Caldera over time scales of months to years.

Use of GNSS

The GNSS, which includes the U.S.-based Global Positioning System (GPS), allows for precise measurement of changes in site positions over timescales of seconds to decades at specific sites (e.g., Bock and Melgar, 2016). In the case of volcanic deformation, GNSS sites are typically used to observe both horizontal and vertical deformation at multiple sites throughout an active region, with greater accuracy and higher temporal resolution than InSAR, but at a much lower spatial density (e.g., Palano et al., 2023).

There are generally two types of GNSS deployments used to measure ground motion. Continuous GNSS sites measure ground deformation over long time periods at permanent observing stations without interruption. In contrast, survey-mode observations can be made using temporary GNSS stations installed for several days at multiple nearby benchmarks in the same area. This allows for spatially denser data at lower temporal resolution. GNSS was not initially created for scientific purposes but has since become the foundation of modern geodesy. This is thanks to its millimeter-level precision and accuracy (Perosanz, 2019). Here, we use survey GNSS observations to measure long-term deformation in the Valles Caldera on decadal time scales.

METHODS AND RESULTS

InSAR Processing Using ISCE

We processed Sentinel-1A data for this region using the open-source InSAR Scientific Computing Environment (ISCE) version 2 (Rosen et al., 2012) on a high-performance computing system maintained by the University of New Mexico Center for Advanced Research Computing.

We downloaded 410 Sentinel-1A scenes covering the Valles Caldera from descending path number 56 from the Alaska Satellite Facility (https://search.asf.alaska.edu/#/; Fig. 1c). A digital elevation model from the SRTM-GL1 dataset (Jain et al., 2018) referenced to the WGS84 ellipsoid was used to remove topographic (parallax) effects from the interferometry. We selected 37 interferograms (which represent a time span of 1 year in order to increase coherence) spanning the time period 2014–2022, after an initial processing of 188 interferograms.

We then applied additional processing steps to the interferograms. To separate primary signals from noise, we applied a Goldstein filter with a strength of 0.5 that utilizes a Fourier transform on each patch of data. We used three azimuth and five range looks (down sampling) to remove speckle noise, and we set the coherence threshold (which determines how similar a pixel is in different SAR observations) at 0.7. The ISCE software creates and executes a series of scripts to process the stack of images, by first identifying where the images overlap, then extracting a valid region and aligning the images precisely, computing and filtering the interferograms and correcting them for topography, merging the separate subswaths (a series of bursts, which are images taken by the satellite) into one image, and unwrapping the final interferograms using the Snaphu algorithm (Chen and Zebker, 2001).

Two of the final interferograms (May 2015–May 2016 and May 2022–May 2023) are given in Figure 2, with phase shown

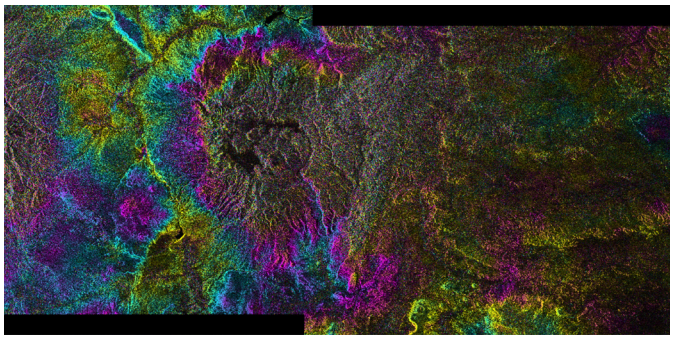

FIGURE 2a. The interferogram of the Valles Caldera created using ISCE version 2 for May 13, 2015, to May 31, 2016. One wavelength is equal to 5.6 cm.

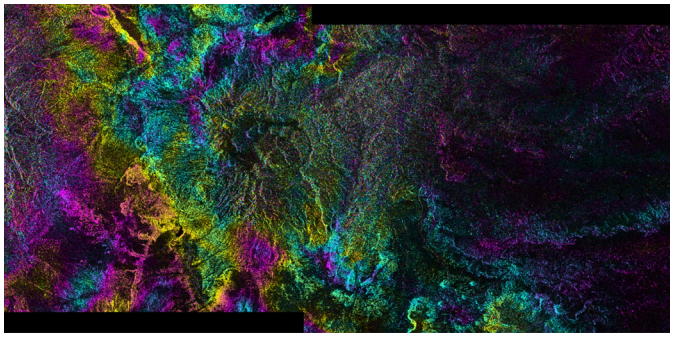

FIGURE 2b. The interferogram of the Valles Caldera created using ISCE version 2 for May 12, 2022, to May 7, 2023. One wavelength is equal to 5.6 cm.

in color and amplitude shown as pixel brightness. The pattern of phase variation in these images reflects mostly atmospheric noise due to humidity, temperature, and pressure changes between the two SAR acquisition dates, and these were accounted for in the later time series analysis. Atmospheric noise appears over small to large wavelengths over the entire interferogram (Foster et al., 2006). After assessing the quality of each interferogram, we used MintPy to create the time series (Yunjun et al., 2019).

Creating Approximately Yearlong Interferograms

To decrease noise levels due to low phase coherence in some images, we used primarily yearlong interferograms and did not process data collected during winter months because snow absorbs most of the radar signal (Fig. 3). We chose interferograms between the months of May and June because these are the time periods least likely to have high amounts of noise due to snowpack or humidity. Choosing only interferograms from dates that are not as highly impacted by these sources of noise can mitigate coherence issues, resulting in a more coherent time series result. These criteria resulted in only 37 usable interferograms.

InSAR Results: LOS Velocities

After inspecting the interferograms to determine whether the region of interest was properly resolved, we ran MintPy to create a time series of the entire time span chosen from the interferograms. This involved reading the unwrapped interferograms, referencing all of them to some chosen reference point, calculating the phase closure, then inverting this into a time series. Atmospheric noise was corrected using the PyAPS component of MintPy, which computes the predicted phase delays using the ERA5 weather model (Hersbach et al., 2020) and removes these predictions from each interferogram. Finally, an image was created showing the line-of-sight (LOS) velocities over the entire time span using a linear fit (Fig. 4). The reference point in this image is the same location as station TA33 (Fig. 7). LOS velocities represent the displacement toward or away from the satellite, with positive values representing uplift or east-southeastward horizontal motion. We estimate the uncertainty is around 1 mm/yr for this type of processing (Havazli and Wdowinski, 2021).

GNSS Processing

In addition to the INSAR data processing, we present preliminary processing of a GNSS campaign survey completed in fall 2022. The collected data include 13 campaign stations first installed and surveyed during October 2002, some of which were also surveyed in 2003, and all of which we resurveyed in 2022. The recent fieldwork involved visiting Valles Caldera in October 2022 and installing six Trimble 5700 GPS receivers with Zephyr Geodetic 1 antennas, using a 13.05-cm spike mount placed directly on the geodetic monuments (Fig. 5). Data were recorded continuously at 30-s intervals. After three

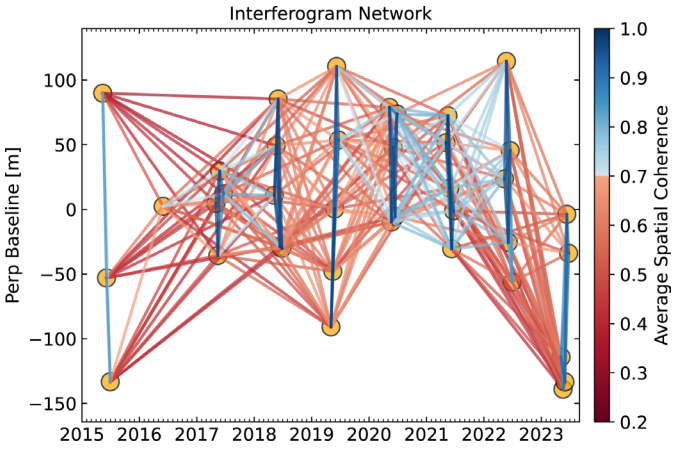

FIGURE 3. A reduced set of approximately yearlong interferograms. The x-axis is time in years, and the y-axis is perpendicular baseline. The lines represent individual interferograms. The dots are SAR acquisitions, and the red lines are interferograms where the majority of the data was unusable due to the spatial coherence being too low; the blue lines represent interferograms with mostly usable data.

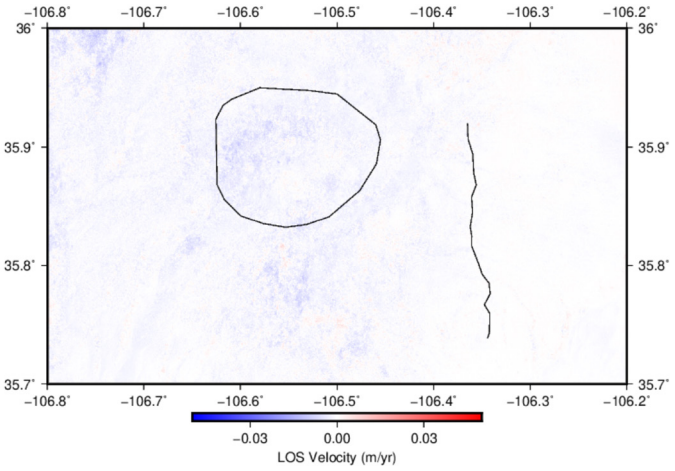

FIGURE 4. Line-of-sight (LOS) velocity over the Valles Caldera created using a linear fit to the MintPy time series from 2014 to 2022. The caldera ring fracture zone, the reference point, and the main break of the Pajarito fault traces are indicated in black.

FIGURE 5. A photograph taken in Valle Seco during the field survey at station VCVS.

to four days, the receivers were collected and redeployed to the remaining benchmarks.

We processed these data using the free software GAMIT (GNSS At MIT) and GLOBK (Global Kalman filter; Herring et al., 2018). When using the double-differencing technique, to precisely determine the coordinates and velocities of the survey GNSS sites, nearby continuous GNSS reference sites must be used. Using the double-difference approach, the atmospheric delays between GPS satellites and the sites can be made to cancel out (assuming the troposphere is the same between each site), allowing determination of the exact distance between these continuous sites and the survey sites. From these "baseline" solutions, the exact coordinates and velocities of the survey sites can then be calculated.

The processing steps were as follows: we converted the raw data into RINEX (Receiver INdependent EXchange) files using the Trimble "Convert to Rinex" software, which provides the GPS observations in a standard ASCII format, usable in our processing steps (Defraigne and Petit, 2003). We then set up a folder with the year we were processing (2002, 2003, and 2022) and downloaded the RINEX files for a set of IGS sites across North America (Figs. 6 and 7). The VCCC survey site was toppled over by an animal during the survey on day 286, so the data for that day and afterward had to be removed during processing. We then ran GAMIT for each group of days, which prepares the data, prepares the batch control, integrates GPS satellite orbits, calculates modeled phase and takes the derivative of that with respect to velocity and position parameters, then estimates parameters using a least-squares technique to create an h-file containing the baseline solutions (distances between sites) for input to GLOBK (Herring et al., 2018). We then used GLOBK to create combined solutions for different years and generate position and velocity solutions for each site. GLOBK uses the known locations and velocities of the IGS sites to estimate precise timeseries and velocities for each survey site within a given reference frame (International Terrestrial Reference Frame 2014 [ITRF2014]). We subtracted the velocity of station TA33 to remove the deformation from the wider region and isolate any deformation from Valles itself (Figs. 7 and 8). We note the results of GPS are preliminary (Figs. 6 and 7). Potential issues with the antenna-spike mount setup used in each campaign are still being evaluated, and other non-secular signals due to surface loading were not considered, meaning the uncertainties are higher than formally reported here. As such, we do not rely on them heavily in the discussion below.

FIGURE 6. Locations of all IGS sites used in the GPS processing. This map was created using Generic Mapping Tools.

DISCUSSION

The InSAR and preliminary GPS results both show limited subsidence across the Valles Caldera and greater region. However, this signal is generally not above the method uncertainties (0.43 mm/yr on average), and no patterns are observed across the entire region including any specific to the caldera. Although neither dataset shows a conclusive deformation source, they are consistent, and both show subsidence. Multiple reasonable hypotheses could explain this based on outside studies and data, and in the following sections we discuss different processes that could explain subsidence in the Valles and the greater region.

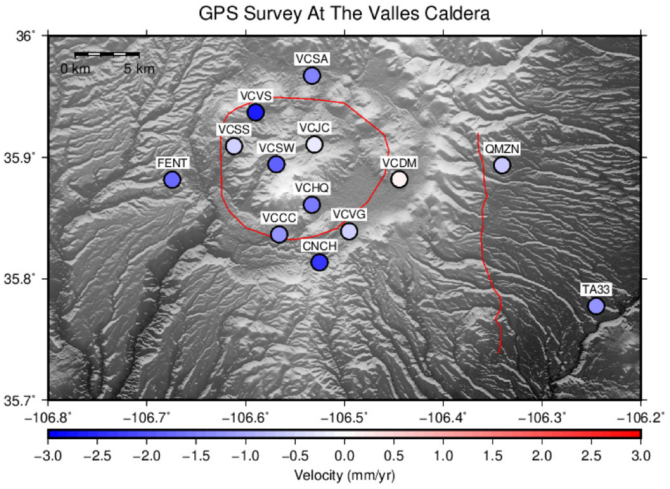

FIGURE 7. The 13 GPS stations processed from 2002 to 2022 with the GLOBK-calculated velocities indicated. The average velocity (vertical deformation) is -1.24 mm/yr. The reference frame used is the International Terrestrial Reference Frame 2014 (IRTF2014).

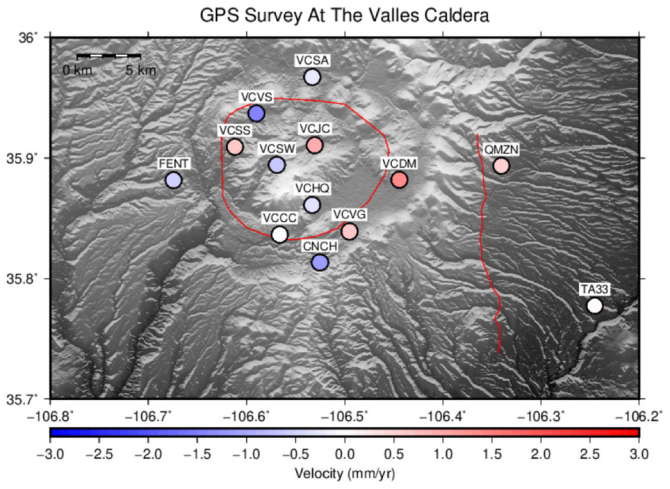

FIGURE 8. The 13 GPS stations processed from 2002 tp 2022 with the GLOBK-calculated velocities indicated, with station TA33 used as a reference station. The average velocity (vertical deformation) is 0.06 mm/yr.

TABLE 1. Site names, occupation start and end dates in GMT time (numbers refer to the Julian date of year 2022), and approximate locations.

GPS Station Name	Day Installed	Day Retrieved	Longitude	Latitude
1. CNCH	276	280	-106.52524	35.81356
2. VCDM	276	280	-106.44443	35.88193
3. VCJC	276	280	-106.53038	35.91059
4. VCSA	276	280	-106.53286	35.96712
5. VCVG	276	280	-106.49529	35.8391
6. VCVS	277	279	-106.58978	35.93701
7. FENT	283	293	-106.67426	35.88151
8. QMZN	293	299	-106.34041	35.89353
9. TA33	291	298	-106.24521	35.77749
10. VCCC	283	293	-106.56604	35.83649
11. VCHQ	283	287	-106.53303	35.86096
12. VCSS	283	293	-106.61173	35.90917
13. VCSW	283	287	-106.56893	35.89426

Fluid Migration

Waite and Smith (2002) argue that recent subsidence in Yellowstone is a result of hydrothermal fluid migration. Valles has a known hydrothermal system that formed around the same time as the caldera itself (Goff and Shevenell, 1987). Parts of this hydrothermal system discharge into the nearby Jemez River, which could cause a subsidence pattern in the region if the discharge rate exceeds recharge from precipitation (Goff and Shevenell, 1987; Goff et al., 1988). If hydrothermal fluid movement is the cause of the surface deformation seen by the geodetic data presented here, it is likely unrelated to the seismically observed low velocity zone (Wilgus et al., 2023), as 10 km is not a reasonable depth for a body of significant hydrothermal fluid (Stimac et al., 2015).

The hydrothermal fluid within the Valles Caldera is also presently degassing (Goff and Janik, 2002; Blomgren et al., 2019), releasing primarily (99%) steam and lesser amounts of CO_2, H_2S, and other geothermal gas components. Degassing also causes the types of vertical motion that we observed (Matthews et al., 1997), and this explanation can potentially explain the regions of the highest subsidence, which are near several springs associated with hydrothermal fluid movement (Figs. 4 and 7).

Magma Crystallization

Observations at Yellowstone suggest that another possible source of subsidence is magma crystallization (Dzurisin et al., 1990). If a shallow magma body is crystallizing beneath the Valles Caldera, it will contract, and it may also have an impact on the movement of groundwater above the crystallized portion of the subjacent pluton (Goff and Grigsby, 1982; Goff et al., 1988). If the magma body is crystalizing, this could also

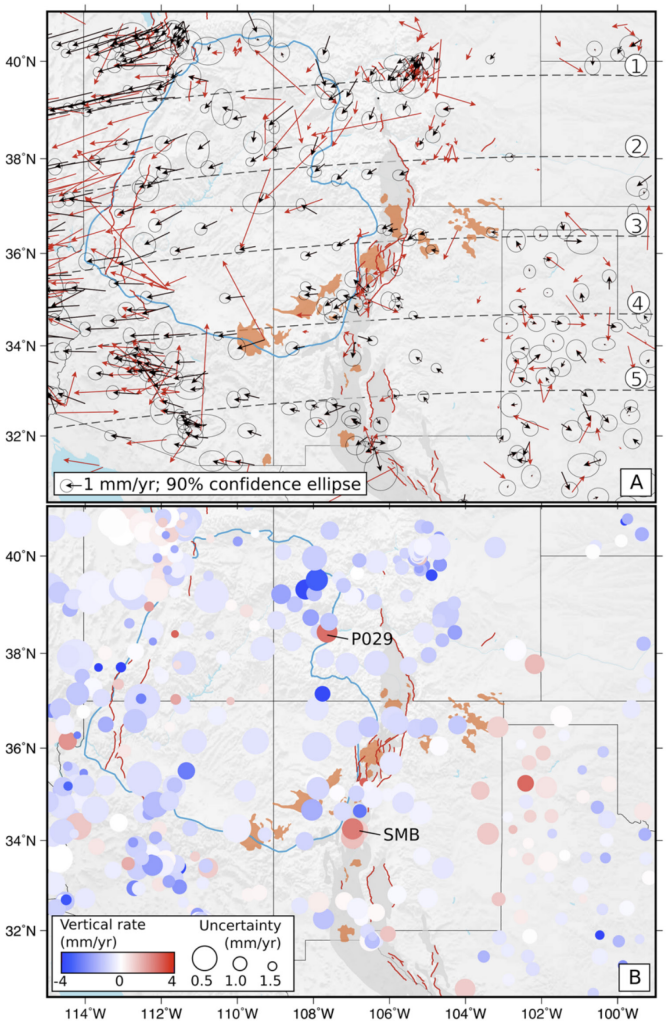

FIGURE 9. GPS processing results from Murray et al. (2019), showing broad subsidence in the Rio Grande rift and Colorado Plateau.

explain why there is both subsidence (cooling magma tends to contract) as well as a seismic low-velocity zone (Roberts et al., 1991), as portions of the magma would still be liquid. However, the imaged low-velocity zone is localized beneath Redondo Peak near the center of the caldera (Wilgus et al., 2023), so subsidence associated with magma crystallization does not explain the broad pattern of observed vertical deformation (Figs. 4 and 8).

Regional Subsidence

The entire region east of the Valles is part of the Rio Grande rift and has been subsiding for the last 25 Myr (Reilinger and York, 1979). Overall, subsidence due to rifting estimated at <1 mm/yr (Fig. 9; Murray et al., 2019) has been observed in the region. This could account for deformation within and around Valles Caldera. More data is needed to determine whether the rates and pattern of subsidence within Valles are significantly greater than and independent of the regional processes.

CONCLUSIONS

In this study, we present new InSAR observations and preliminary GNSS results within the Valles Caldera spanning the last several decades. The total rates of deformation seen in both InSAR and GNSS results are consistent and show limited subsidence, but they are also small and within measurement error. The GNSS data have a 19-year gap in the observations between 2003 and 2022, limiting our ability to detect any variations in the rates of motion. Our InSAR observations are derived from yearlong interferograms to reduce seasonal effects but still include some noise due to the high topography and dense vegetation within Valles. Although additional geodetic observations are needed to better resolve the deformation field, previous work suggests both hydrothermal and regional tectonic processes could influence deformation patterns in the region.

Currently, no continuous GPS stations are available within the general region. In the future, installation of continuous stations within the Valles Caldera would enable better monitoring, especially in regions of suspected high hydrothermal fluid movement and around Redondo Peak, which is near the inferred magma body. Our results do not show significant deformation; however, observations from the better-monitored Yellowstone and Long Valley Calderas do indicate change is possible on decadal timescales (Dzurisin et al., 1990). Thus, continuous monitoring would help refine our understanding of the Valles system and its contemporary state in northern New Mexico.

ACKNOWLEDGMENTS

This article benefited from the helpful reviews of Fraser Goff (New Mexico Tech) and Jeng Hann Chong (University of New Mexico). The work done in this study was made possible by the University of New Mexico Center for Advanced Research Computing. Data collection for the GNSS observations was funded by the Los Alamos National Laboratory Nuclear Safety Office as part of the Los Alamos Seismic Hazards program, and this paper was released under LA-UR-24-22919.

REFERENCES

Bamler, R., and Hartl, P., 1998, Synthetic aperture radar interferometry: Inverse Problems, v. 14, R1, https://doi.org/10.1088/0266-5611/14/4/001

Bekaert, D.P.S., Walters, R.J., Wright, T.J., Hooper, A.J., and Parker, D.J., 2015, Statistical comparison of InSAR tropospheric correction techniques: Remote Sensing of Environment, v. 170, p. 40–47, https://doi.org/10.1016/j.rse.2015.08.035

Block, G.A., Roy, M., Graves, E., and Grapenthin, R., 2023, Pressurizing magma within heterogeneous crust: A case study at the Socorro magma body, New Mexico, USA: Geophysical Research Letters, v. 50, no. 20, https://doi.org/10.1029/2023GL105689

Blomgren, V.J., Crossey, L.J., Karlstrom, K.E., Fischer, T.P., and Darrah, T.H., 2019, Hot spring hydrochemistry of the Rio Grande rift in northern New Mexico reveals a distal geochemical connection between Valles Caldera and Ojo Caliente: Journal of Volcanology and Geothermal Research, v. 387, 106663, https://doi.org/10.1016/j.jvolgeores.2019.106663

Bock, Y., & Melgar, D., 2016, Physical applications of GPS geodesy: a review: Reports on Progress in Physics, v. 79, no. 10, pp. 106801, https://doi.org/10.1088/0034-4885/79/10/106801

Bock, Y., Nikolaidis, R., de Jonge, P., and Bevis, M., 2000, Instantaneous geodetic positioning at medium distances with the Global Positioning System: Journal of Geophysical Research: Solid Earth, v. 105, no. B12, p. 28223–28253, https://doi.org/10.1029/2000JB900268

Berglund, H.T., Sheehan, A.F., Murray, M.H., Roy, M., Lowry, A.R., Nerem, R.S., & Blume, F., 2012, Distributed deformation across the Rio Grande Rift, Great Plains, and Colorado Plateau: Geology, v. 40, no. 1, p. 23–26, https://doi.org/10.1130/G32418.1

Chen, C., and Zebker, H., 2001, Two-dimensional phase unwrapping with use of statistical models for cost functions in nonlinear optimization: Journal of the Optical Society of America A, v. 18, no. 2, p. 338–351, https://doi.org/10.1364/JOSAA.18.000338

Defraigne, P., and Petit, G., 2003, Time transfer to TAI using geodetic receivers: Metrologia, v. 40, no. 4, https://doi.org/10.1088/0026-1394/40/4/307

Dzurisin, D., Savage, J., and Fournier, R., 1990, Recent crustal subsidence at Yellowstone Caldera, Wyoming: Bulletin of Volcanology, v. 52, no. 4, p. 247–270, https://doi.org/10.1007/BF00304098

Fialko, Y., & Simons, M., 2001, Evidence for on□going inflation of the Socorro Magma Body, New Mexico, from interferometric synthetic aperture radar imaging: Geophysical Research Letters, v. 28, no. 18, p. 3549–3552, https://doi.org/10.1029/2001GL013318

Foster, J., Brooks, B., Cherubini, T., Shacat, C., Businger, S., and Werner, C.L., 2006, Mitigating atmospheric noise for InSAR using a high resolution weather model: Geophysical Research Letters, v. 33, no. 16, https://doi.org/10.1029/2006GL026781

Goff, F., 2010, The Valles Caldera: New Mexico's supervolcano: New Mexico Earth Matters, v. 10, no. 1, p. 1–4.

Goff, F., and Grigsby, C.O., 1982, Valles Caldera geothermal systems, New Mexico, U.S.A.: Journal of Hydrology, v. 56, no. 1–2, p. 119–136.

Goff, F., and Janik, C.J., 2002, Gas geochemistry of the Valles Caldera region, New Mexico and comparisons with gases at Yellowstone, Long Valley and other geothermal systems: Journal of Volcanology of Geothermal Research, v. 116, p. 299–323, https://doi.org/10.1016/S0377-0273(02)00222-6

Goff, F., and Kelley, S.A., 2021, Facts and hypotheses regarding the Miocene-Holocene Jemez lineament, New Mexico, Arizona, and Colorado, *in* Frey, B.A., Kelley, S.A., Zeigler, K.E., McLemore, V.T., Goff, F., and Ulmer-Scholle, D.S., eds., Geology of the Mount Taylor Area: New Mexico Geological Society Guidebook 71, p. 101–115.

Goff, F., and Shevenell, L., 1987, Travertine deposits of Soda Dam, New Mexico, and their implications for the age and evolution of the Valles caldera hydrothermal system: Geological Society of America Bulletin, v. 99, p. 292–302, https://doi.org/10.1130/0016-7606(1987)99<292:TDOSD-N>2.0.CO;2

Goff, F., Shevenell, L., Gardner, J.N., Vuataz, F.-D., and Grigsby, C.O., 1988, The hydrothermal outflow plume of Valles caldera, New Mexico, and a comparison with other outflow plumes: Journal of Geophysical Research, v. 93, p. 6041–6058, https://doi.org/10.1029/JB093iB06p06041

Goff, F., Gardner, J.N., Reneau, S.L., Kelley, S.A., Kempter, K.A., and Lawrence, J.R., 2011, Geologic map of the Valles caldera, Jemez Mountains, New Mexico: New Mexico Bureau of Geology and Mineral Resources Geologic Map 79, scale 1:50,000, 30 p.

Grapenthin, R., Cheng, Y., Angarita, M., Tan, D., Meyer, F. J., Fee, D., and Wech, A., 2022, Return from dormancy: Rapid inflation and seismic unrest driven by transcrustal magma transfer at Mt. Edgecumbe (L'úx Shaa) Volcano, Alaska: Geophysical Research Letters, v. 49, no. 20, https://doi.org/10.1029/2022GL099464

Havazli, E., and Wdowinski, S., 2021, Detection threshold estimates for InSAR time series: A simulation of tropospheric delay approach: Sensors, v. 21, no. 4, 1124, https://doi.org/10.3390/s21041124

Heiken, G., Goff, F., Gardner, J., Baldridge, W., Hulen, J., Nielson, D., and Vaniman, D., 1990, The Valles/Toledo Caldera Complex, Jemez Volcanic Field, New Mexico: Annual Review of Earth and Planetary Sciences, v. 18, no. 1, p. 27–53.

Herring, T., King, R., and McClusky, S., 2018, GPS analysis at MIT: Reference Manual 10.6: Cambridge, MA, Massachusetts Institute of Technology.

Hersbach, H., Bell, B., Berrisford, P., Hirahara, S., Horányi, A., Muñoz□Sabater, J., Nicolas, J., Peubey, C., Radu, R., Schepers, D., and Simmons, A., 2020, The ERA5 global reanalysis: Quarterly Journal of the Royal Meteorological Society, v. 146, no. 730, p. 1999–2049.

Jain, A., Thaker, T., Chaurasia, A., Patel, P., and Singh, A., 2018, Vertical accuracy evaluation of SRTM-GL1, GDEM-V2, AW3D30 and CartoDEM-V3.1 of 30-m resolution with dual frequency GNSS for lower Tapi Basin India: Geocarto International, v. 33, no. 11, p. 1237–1256, https://doi.org/10.1080/10106049.2017.1343392

Kelley, S.A., McIntosh, W.C., Goff, F., Kempter, K.A., Wolff, J.A., Esser, R., Brascheyko, S., Love, D., and Gardner, J.N., 2013, Spatial and temporal trends in pre-caldera Jemez Mountains and volcanic and fault activity: Geosphere, v. 9, p. 614–646, https://doi.org/10.1130/GES00897.1

Liang, C., Agram, P., Simons, M., and Fielding, E.J., 2019, Ionospheric correction of InSAR time series snalysis of C-band Sentinel-1 TOPS data: IEEE Transactions on Geoscience and Remote Sensing, v. 57, no. 9, p. 6755–6773, https://doi.org/10.1109/TGRS.2019.2908494

Lu, Z., and Dzurisin, D., 2014, InSAR Imaging of Aleutian Volcanoes: Monitoring a Volcanic Arc from Space: Berlin, Springer, 390 p, https://doi.org/10.1007/978-3-642-00348-6_6

Massonnet, D., Briole, P., and Arnaud, A., 1995, Deflation of Mount Etna monitored by spaceborne radar interferometry: Nature, v. 375, no. 6532, p. 567–570, https://doi.org/10.1038/375567a0

Matthews, S.J., Gardeweg, M.C., and Sparks, R.S.J., 1997, The 1984 to 1996 cyclic activity of Lascar Volcano, northern Chile: Cycles of dome growth, dome subsidence, degassing and explosive eruptions: Bulletin of Volcanology, v. 59, no. 1, p. 72–82, https://doi.org/10.1007/s004450050176

Murray, K.D., Murray, M.H., and Sheehan, A.F., 2019, Active deformation near the Rio Grande rift and Colorado Plateau as inferred from continuous Global Positioning System measurements: Journal of Geophysical Research: Solid Earth, v. 124, no. 2, p. 2166–2183, https://doi.org/10.1029/2018JB016626

Nasholds, M.W.M., and Zimmerer, M.J., 2022, High-precision $^{40}Ar/^{39}Ar$ geochronology and volumetric investigation of volcanism and resurgence following eruption of the Tshirege Member, Bandelier Tuff, at the Valles Caldera: Journal of Volcanology and Geothermal Research, v. 431, 107624, https://doi.org/10.1016/j.jvolgeores.2022.107624/

Palano, M., Calcaterra, S., Gambino, P., Porfidia, B., and Sparacino, F., 2023, GNSS-based long-term deformation at Mount Etna volcano (Italy): Results in Geophysical Sciences, v. 14, 100056, https://doi.org/10.1016/j.ringps.2023.100056

Perosanz, F., 2019, GNSS: A revolution for precise geopositioning: Comptes Renfus Physique, v. 20, no. 3, p. 171–175, https://doi.org/10.1016/j.crhy.2019.05.018

Poland, M., and Zebker, H., 2022, Volcano geodesy using InSAR in 2020: The past and next decades: Bulletin of Volcanology, v. 84, no. 3, https://doi.org/10.1007/s00445-022-01531-1

Reilinger, R., and York, J., 1979, Relative crystal subsidence from leveling data in a seismically active part of the Rio Grande rift, New Mexico: Geology, v. 7, no. 3, p. 139–143, https://doi.org/10.1130/0091-7613(1979)7<139:RCSFLD>2.0.CO;2

Roberts, P.M., Aki, K., and Fehler, M.C., 1991, A low□velocity zone in the basement beneath the Valles Caldera, New Mexico: Journal of Geophysical Research: Solid Earth, v. 96, no. B13, p. 21583–21596, https://doi.org/10.1029/91JB02048

Rosen, P.A., Gurrola, E., Sacco, G.F., and Zebker, H., 2012, The InSAR scientific computing environment: EUSAR 2012–9th European conference on synthetic aperture radar.

Spell, T., McDougall, I., and Doulgeris, A., 1996, Cerro Toledo Rhyolite, Jemez volcanic field, New Mexico: Ar geochronology of eruptions between two caldera-forming events: Geological Society of America Bulletin, v. 108, p. 1549–1566, https://doi.org/10.1130/0016-7606(1996)108%3C1549:CTRJVF%3E2.3.CO;2

Steck, L.K., Thurber, C.H., Fehler, M.C., Lutter, W.J., Roberts, P.M., Baldridge, W.S., Stafford, D.G., and Sessions, R., 1998, Crust and upper mantle P wave velocity structure beneath Valles Caldera, New Mexico: Results from the Jemez teleseismic tomography experiment: Journal of Geophysical Research: Solid Earth, v. 103, no. B10, p. 24301–24320, https://doi.org/10.1029/98JB00750

Stimac, J.A., Goff, F., and Goff, C.J., 2015, Intrusion-related geothermal systems, *in* Sigurdsson, H., Houghton, B, McNutt, S, Rymer, H., and Stix, J., eds., The Encyclopedia of Volcanoes (second edition): Amsterdam, Elsevier, p. 799–822, https://doi.org/10.1016/B978-0-12-385938-9.00046-8

Suhr, G., 1981, Seismic crust anomaly under the Valles caldera in New Mexico, USA [Unpublished consultant report]: Hanover, Germany, PRAKLA-SEISMOS GMBH, 56 p.

Tizzani, P., Berardino, P., Casu, F., Euillades, P., Manzo, M., Ricciardi, G., Zeni, G., and Lanari, R., 2007, Surface deformation of Long Valley Caldera and Mono Basin, California, investigated with the SBAS-InSAR approach: Remote Sensing of Environment, v. 108, no. 3, p. 277–289, https://doi.org/10.1016/j.rse.2006.11.015

Treuhaft, R.N., Madsen, S.N., Moghaddam, M., and van Zyl, J.J., 1996, Vegetation characteristics and underlying topography from interferometric radar: Radio Science, v. 31, no. 6, p. 1449–1485, https://doi.org/10.1029/96RS01763

van Wijk, J., Koning, D., Axen, G., Coblentz, D., Gragg, E., and Sion, B., 2018, Tectonic subsidence, geoid analysis, and the Miocene-Pliocene unconformity in the Rio Grande rift, southwestern United States: Implications for mantle upwelling as a driving force for rift opening: Geosphere, v. 14, no. 2, p. 684–709, https://doi.org/10.1130/GES01522.1

Vasco, D.W., Puskas, C.M., Smith, R.B., and Meertens, C.M., 2007, Crustal deformation and source models of the Yellowstone volcanic field from geodetic data: Journal of Geophysical Research: Solid Earth, v. 112, no. B7, https://doi.org/10.1029/2006JB004641

Waite, G., and Smith, R., 2002, Seismic evidence for fluid migration accompanying subsidence of the Yellowstone caldera: Journal of Geophysical Research: Solid Earth, v. 107, no. B9, p. ESE 1-1–1-15, https://doi.org/10.1029/2001JB000586

Wannamaker, P. E., 1997, Tensor CSAMT survey over the Sulphur Springs thermal area, Valles Caldera, New Mexico, United States of America, Part I: Implications for structure of the western caldera: Geophysics, v. 62, no. 2, p. 451–465, https://doi.org/10.1190/1.1444156

Wilgus, J., Schmandt, B., Maguire, R., Jiang, C., and Chaput, J., 2023, Shear velocity evidence of upper crustal magma storage beneath Valles Caldera: Geophysical Research Letters, v. 50, no. 5, e2022GL101520, https://doi.org/10.1029/2022GL101520

Wolff, J., and Gardner, J., 1995, Is the Valles caldera entering a new cycle of activity?: Geology, v. 23, no. 5, p. 411–414, https://doi.org/10.1130/0091-7613(1995)023%3C0411:ITVCEA%3E2.3.CO;2

Wolff, J., Brunstad, K., and Gardner, J., 2011, Reconstruction of the most recent volcanic eruptions from the Valles Caldera, New Mexico: Journal of Volcanology and Geothermal Research, v. 199, no. 1–2, p. 53–68, https://doi.org/10.1016/j.jvolgeores.2010.10.008

Wright, T.J., Parsons, B.E., and Lu, Z., 2004, Toward mapping surface deformation in three dimensions using InSAR: Geophysical Research Letters, v. 31, no. 1, https://doi.org/10.1029/2003GL018827

Yunjun, Z., Fattahi, H., and Amelung, F., 2019, Small baseline InSAR time series analysis: Unwrapping error correction and noise reduction: Computers & Geosciences, v. 133, 104331, https://doi.org/10.1016/j.cageo.2019.104331

Zimmerer, M., Lafferty, J., and Coble, M., 2016, The eruptive and magmatic history of the youngest pulse of volcanism at the Valles Caldera: Implications for successfully dating late Quaternary eruptions: Journal of Volcanology and Geothermal Research, v. 310, p. 50–57, https://doi.org/10.1016/j.jvolgeores.2015.11.021

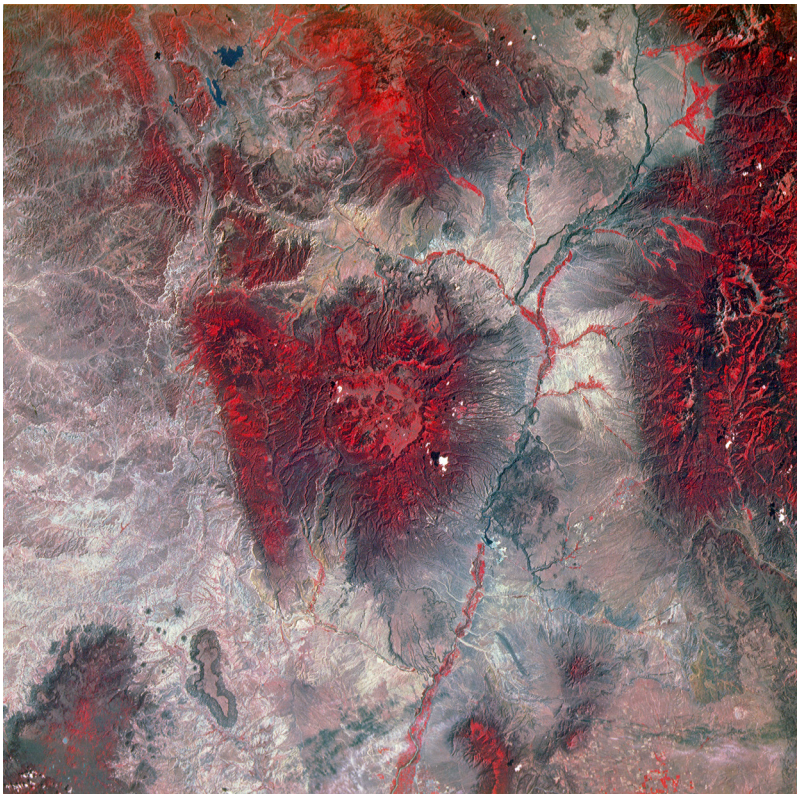

False-color Landsat image showing the Nacimiento Mountains and Valles Caldera (https://solarviews.com/cap/volc/valles1.htm#google_vignette). Reed et al. (2024) suggest that the similar north-south dimensions of the Nacimiento Mountains and Valles Caldera may reflect Quaternary uplift of the Jemez Mountains volcanic field at the million year time scale that drove reactivation of the range-bounding Nacimiento fault. Devine et al. (2024) did not find a geodetic signal of uplift in or around the Valles Caldera in the past 20 years.